ELSEVIER

Journal of Power Sources 110 (2002) 389–400

JOURNAL OF POWER SOURCES

www.elsevier.com/locate/jpowsour

# From molecular models to system analysis for lithium battery electrolytes

John B. Kerr*, Steven E. Sloop, Gao Liu, Yong Bong Han, Jun Hou, Shanger Wang

*Lawrence Berkeley National Laboratory, MS 62-203, 1 Cyclotron Road, Berkeley, CA 94720, USA*

**Abstract**

The behavior of polymer electrolytes in lithium batteries is reviewed in the context of molecular scale models as well as on the system scale. It is shown how the molecular structure of the electrolyte strongly influences ion transport through the polymer as well as across the interfaces and determines the values of a number of parameters needed for system models that can predict the performance of the battery (e.g. $\kappa$, $D$, $t_0^+$ and $i_0$). The interaction of the electrolyte with the electrodes not only leads to transfer of the lithium ion across the interface but also to side reactions that profoundly influence the calendar and life cycle of the battery. Typically these electrochemically induced side reactions generate the SEI layer, but inherent instability of the bulk electrolyte may also play a role in the formation of surface layers. These various reactions can lead to changes in the mechanical properties of the separator and electrode structure that promote life-limiting phenomena such as dendrite growth, passivation and morphology changes. The rheological model of Eisenberg is drawn upon to show how the interactions of the electrolyte with surfaces can lead to distinct changes in mechanical and transport properties that may limit the battery performance and lead to diminished performance with time. The molecular level models may be combined with the rheological models to provide workable models of the interfaces and bulk electrolyte dynamics that in turn can be used to provide a more accurate level of performance prediction from the system models. This connects molecular structure with battery performance and guides the design and synthesis of new and better materials.


*Keywords:* Lithium battery; Polymer electrolytes; SEI layer; Molecular models; System models; Rheological models; Ion solvation; Mobility

## 1. Introduction

In any rechargeable lithium battery three main processes must occur. The lithium ions must reversibly transfer to and from the anode at or near 0 V versus Li, the lithium ions must be transported across the separator at rates sufficiently high to support the needed power demand and they must transfer to and from the cathode structure in a reversible fashion at the highest possible potential relative to the lithium anode. These processes should occur with a minimum of inefficient side reactions and the components of the cell should be chemically, thermally and mechanically stable for the duration of the battery life. Each of these processes may be modeled at a molecular level as well as intermediate morphological and rheological levels and a goal is to develop a system model that correctly predicts the behavior of the battery while incorporating the results of the molecular, rheological and morphological models. Realization of this goal would allow a more direct and useful connection between materials design and ultimate battery performance.

The design, synthesis and testing of polymer electrolytes for lithium metal polymer batteries [1,2] presents a good example of how the molecular level models may be appropriately linked to system models. In general, molecular models target phenomena that occur on the femtosecond [3,4] time-scale for electron transfer to pico- and nanoseconds for chemical reactions or ion transport [5–8] while system models deal with time-scales that range from seconds to hours [9–12]. Even more daunting is the prospect of linking these time-scales with models to predict calendar and lifetimes cycle which can span years. However, the science of rheology has already developed methods to span such very different time-scales and to translate the effects of molecular scale changes into macroscopic and long term changes [13,14]. To fully take advantage of these possibilities, it is necessary to develop materials designed to test the models and provide a means to validate the predictions. It is the purpose of this paper to describe some initial efforts in the design of new polymers that may test some of the molecular level hypotheses and also provide connections to the macroscale and system-level models.

## 2. Experimental

General procedures and equipment for the preparation and testing of polymer electrolytes have been previously

* Corresponding author.
*E-mail address:* jbkerr@lbl.gov (J.B. Kerr).

0378-7753/02/$ – see front matter 
PII: S0378-7753(02)00202-1

described [15]. Transport properties ($\sigma$, $D_s$ and $t_0^+$) were measured according to the method of Newman and co-workers [16,17]. Mechanical properties were measured using a Rheometrics R800 rheometer. Preparation of the various polymers has been previously described for monomers containing ethylene oxide units [15,18,19]. Polymers containing the trimethylene link between two oxygen atoms were derived from 1,3-propanediol to prepare the monomers and the monomers were polymerized by the same general procedures. A typical example of the synthetic procedure is given below. Cross-linking of polymer membranes was accomplished by a variation of the method described by Allcock et al. [20].

### 2.1. Preparation of $PE(TMO)_3$

#### 2.1.1. Monomer synthesis (Fig. 6)

*2.1.1.1. 2-(2,6-Dioxanonan-9-oxy)tetrahydropyran [$CH_3$-($OCH_2CH_2CH_2)_2OTHP$] (**3**).* 2-Oxapentan-5-ol (**1**) (14.0 g, 0.210 mol), **2** (28.0 g, 0.156 mol) and tetrabutylamonium hydrogen sulfate (5.0 g, 0.015 mol) were mixed with 50% sodium hydroxide aqueous solution (75 ml) and toluene (50 ml). The mixture was heated to 70 °C and mechanically stirred overnight. The mixture was poured into 50 g of crushed ice and extracted with ether (50 ml × 3). The organic layers were combined and washed with saturated NaCl aqueous solution (20 ml × 2) and concentrated under reduced pressure. The residue oil was vacuum distilled at 2–5 Torr in a 120 °C oil bath to remove volatile reactants. The residue brownish oil (25.5 g) in the pot was the crude product. Yield: 65%, 88% purity by GC analysis.

*2.1.1.2. 2,6-Dioxanonan-9-ol [$CH_3(OCH_2CH_2CH_2)_2OH$] (**4**).* Two molar HCl aqueous solution (10 ml) was added to an ethanol solution (100 ml) of crude 2-(2,6-dioxanonan-9-oxy)tetrahydropyran (**3**) (20.5 g). The mixture was refluxed for 5 h, neutralized with small amount of $NaHCO_3$ powder and concentrated under reduced pressure. The residue oil was vacuum distilled at in 90 °C/2 Torr to yield 15.0 g final product. Yield: 85%, 95% purity by GC.

*2.1.1.3. 2-(2,6,10-Trioxaunidecan-13-oxy)tetrahydropyran [$CH_3(OCH_2CH_2CH_2)_3OTHP$] (**5**).* The crude product was obtained as described for **3** above as a brownish oil in 77% yield.

*2.1.1.4. 2,6,10-Trioxaunidecan-13-ol [$CH_3(OCH_2CH_2CH_2)_3OH$] (**6**).* The crude product was obtained as described for **4** as a brownish oil. It was then distilled at 4 Torr in 100 °C oil bath to remove the volatiles. The residue oil in the pot was used in the next step without further purification. Crude yield: 100%.

*2.1.1.5. l,2-Epoxy-4,8,12,16-tetraoxyheptdecane [$EPOCH_2O(CH_2CH_2CH_2O)_3CH_3$] (**7**).* 2,6,10-Trioxaunidecan-13-ol (**6**) (crude 20 g, 66% purity, 0.064 mol), epichlorohydrin (50 ml, 0.64 mol) and tetrabutylamonium hydrogen sulfate (8.0 g, 0.024 mol) were mixed with 50% sodium hydroxide aqueous solution (100 ml). The mixture was mechanically stirred at room temperature for 5 h. The mixture was poured into 50 g of crashed ice and extracted with ether (50 ml × 3). The organic layers were combined, washed with saturated NaCl aqueous solution (20 ml × 2), dried over $MgSO_4$, filtered and concentrated at reduced pressure. The residue oil was vacuum distilled at 95 °C/0.1 Torr from a 180 °C oil bath. The product was collected and fractionally distilled twice more. Ten gram of final product was collected. Yield: 66%, 96% purity by GC analysis.

#### 2.1.2. Polymerization of **7** to form $PE(TMO)_3$ (Fig. 7)

The polymerization was performed in a dry box. $EPOTMO_3$ purified monomer (4.5 g, 17 mmol) together with allyl glycidyl ether (0.10 ml, 0.86 mmol) (5% to monomer) was stirred and preheated to 65 °C. One molar THF solution of potassium *t*-butoxide (0.34 ml) (2% to monomer) was added to the stirred mixture. The mixture turned yellow instantly. The polymerization was allowed to go for 4 h, during which the color of the mixture changed from yellow into light brown and the mixture became more and more viscous until the magnetic stir bar stopped. The polymerization was quenched by adding small amount of methanol out side of the dry box. The sticky polymer was dissolved in methylene chloride (30 ml) and washed with 15 ml of water. The organic layer was concentrated under reduce pressure to give 4.4 g of light yellow sticky polymer. The polymer was fractionated by dissolution in THF and precipitation with hexane three times to give 3.9 g of near colorless transparent resin. Yield: 87%. GPC analysis gave $M_w$: 28000, PDI: 2.6.

## 3. Results and discussion

### 3.1. Effect of polymer structure

In a previous publication [15], the performance in lithium batteries was described for a number of polymer electrolytes containing lithium bis(trifluoromethylsulfonyl)imide salt (LiTFSI). The polymers were linear or comb branch structures based on ethylene oxide units that solvate the lithium ions. It was noted that the conductivities of the various electrolytes depended upon the polymer architecture particularly at temperatures below 25 °C. Above this temperature, the conductivities did not vary significantly provided that the number of ethylene oxide units that connected the polymer structural groups was larger than five. The typical structural groups were acrylate, propylene oxide, oxymethylene or polystyrene and the materials were all completely amorphous when mixed with LiTFSI. The conductivities of two comb branch polymers, polyepoxide ether ($PEPE_5$) and polyvinyl ether ($PVE_5$) are plotted against $1/T$ in Fig. 1

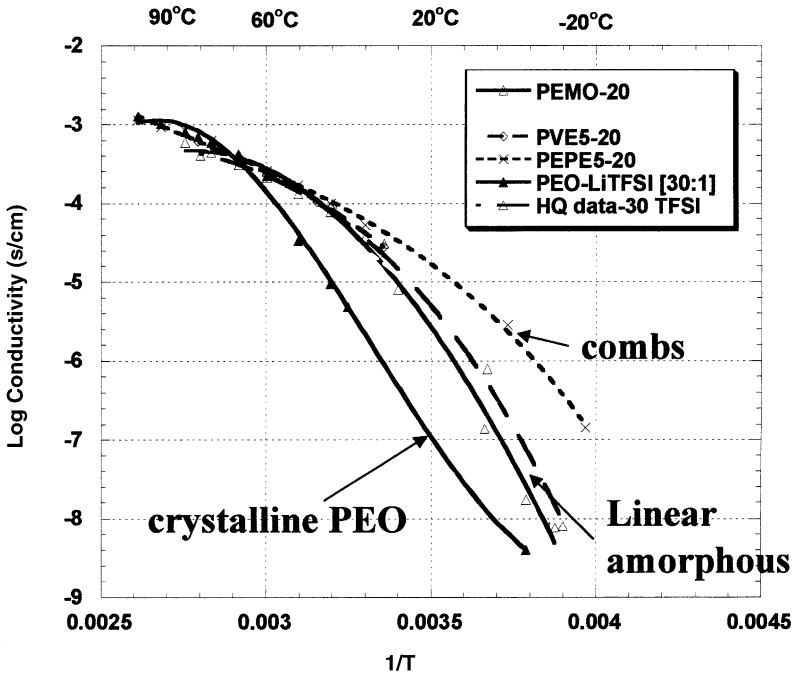


Fig. 1. Conductivities of linear and comb branch polymer electrolytes with LiTFSI salt (20:1 O:Li ratio) plotted against I/$T$(K). PEMO: oxymethylene linked PEG400; PEO: polyethylene oxide; HQ data is data obtained from [22] for a co-polymer of ethylene oxide and propylene oxide; $PVE_5$ and $PEPE_5$ are polyvinyl ether and polyepoxide ether comb branches, respectively, with five ethylene oxide units in the side chains.

together with the conductivities of oxymethylene linked PEG400 (PEMO), [21] PEO and an amorphous ethylene oxide–propylene oxide co-polymer reported by HydroQuebec (HQ) as a useful polymer for electric vehicle battery use [22,23]. The crystalline PEO electrolyte exhibits a lower conductivity than the linear amorphous polymers below its melting point of ∼60 °C [24], while the linear amorphous polymers exhibit much poorer conductivities than the comb materials below 30 °C. This latter effect appears to be due to the extra degree of freedom inherent to the comb materials rather than any crystallinity in the linear polymers as had been previously thought. [15]

Above 60 °C the conductivities of all the polymers converge so that there is no conductivity advantage of the combs or co-polymers over the inexpensive PEO polymer in this temperature range. The transport properties of high molecular weight, PEO–LiTFSI electrolytes at 85 °C have been reported [25]. They are similar to the values found for PEMO–LiTFSI at 85 °C [17]. The salt diffusion coefficients, $D_s$, and transference numbers, $t_0^+$, for PEMO–LiTFSI are shown as a function of salt concentration and temperature in Fig. 2. Full details of the measurements will be published elsewhere. These values have been used to model the behavior of a $Li/V_6O_{13}$ cell and the results showed clearly that the energy and power densities obtained at 40 °C were inadequate for electric vehicle use [9]. The transport properties measured at 85 °C give more satisfactory results but both power and energy densities were still lower than those reported for commercial prototypes [26] and the stated goals of the US Advanced Battery Consortium for EV use [27]. It was found that the size of the anode resistance had a considerable influence on the power and energy density and by suitable adjustment of this parameter and the cathode voltage the model correctly estimated the performance of the prototype batteries at 85 °C. The transport properties measured at 60 °C indicate that the battery would not meet the requirements of EV use and the effects of the electrode resistance are even more pronounced at this lower temperature.

It is of interest to note that the salt diffusion coefficients reported here for PEMO–LiTFSI are similar to those of the HQ co-polymer and the conductivities also match quite closely (Fig. 1). Similarly, the transport properties of PEMO–LiTFSI have been used to correctly predict the transition time behavior of $PEPE_2$–LiTFSI electrolytes as a function of temperature (85 and 75 °C) in symmetrical lithium/lithium cells (transition time experiments involve passing current at or above the limiting current until the concentration of lithium ions at the negative electrode reaches zero). These results indicate that the transport properties for the comb materials are similar to those measured for PEMO, at least above 30 °C. The higher conductivities of the comb materials at low temperatures derive from the extra mobility of the side chains which have one end free.

Such results are consistent with current models of the mechanisms of ionic motion through "dry" polymers [5–8,28–32]. Fig. 3 shows a scheme that is meant to illustrate the concepts and is by no means entirely precise. Two processes are envisioned that may limit the ionic motion.

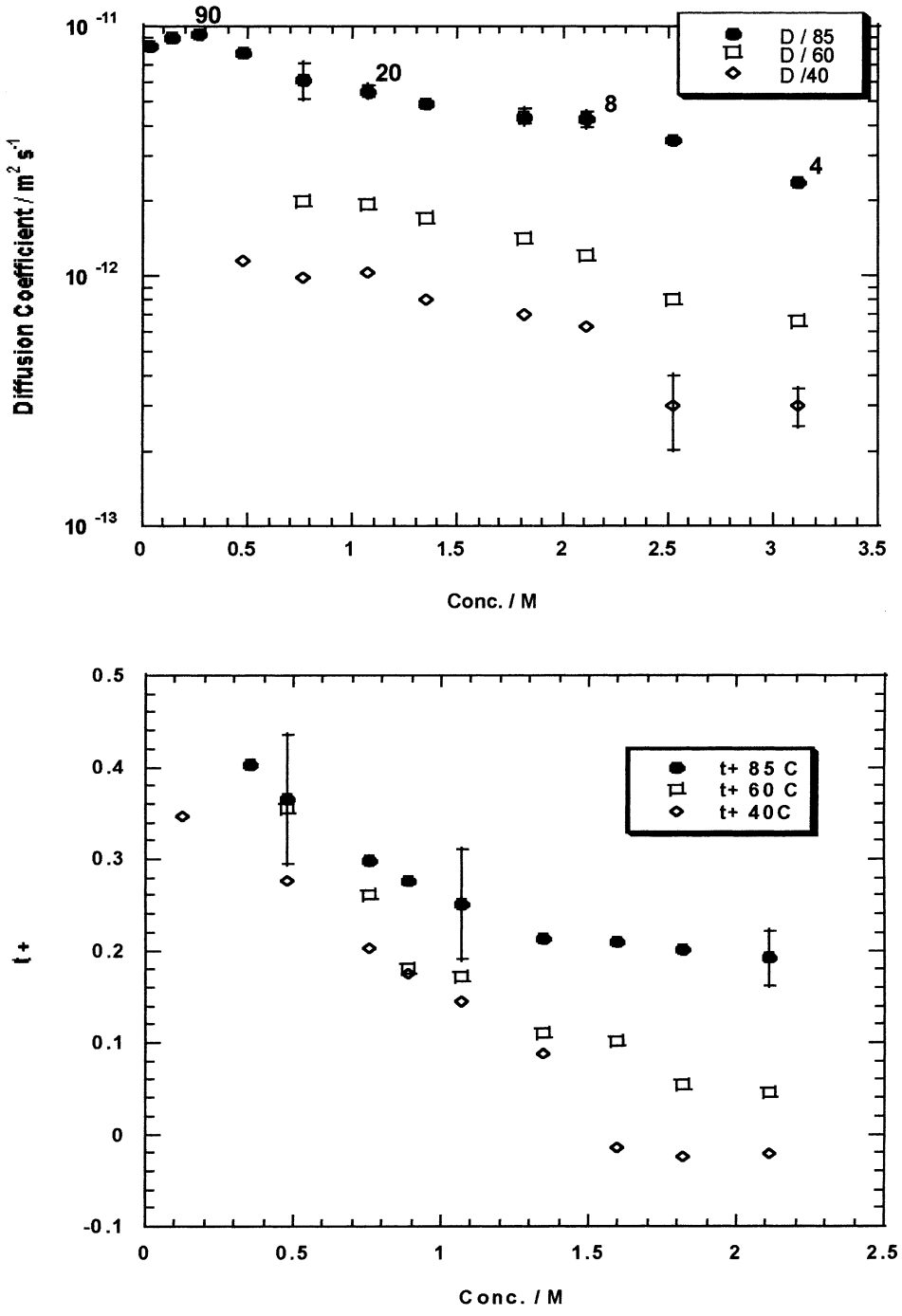


Fig. 2. Salt diffusion coefficients ($D_s$) and transference numbers ($t_0^+$) for PEMO plotted as a function of concentration (mol/l) for three different temperatures: 85, 60 and 40 °C. Numbers on diffusion coefficient curve are O:Li ratios.

One involves the segmental motion of the polymer chain and is represented by the exaggerated swinging motion in Fig. 3. Generally this is related to the glass transition temperature, $T_g$ and as the motion is greater the more the operating temperature is above $T_g$. Motion like this is quite consistent with the observed higher conductivities of the comb materials, which have an untethered chain end and which can be less dependent on the $T_g$. The second type of motion is represented in Fig. 3 by the motion of the lithium ion from one chain to another, which is under Arrhenius control and related to solvation considerations. Fig. 4 illustrates the energetics of the transfer of the lithium ion from one site to another. The nature of the groups involved in the solvation will control this motion and a variety of these are listed in the figure. Strong binding of the lithium ion, as would occur with carbonate or acrylate groups will increase the depth of the energy wells that the ion sits in. The height of the energy barrier will depend on the nature of the transition state. This

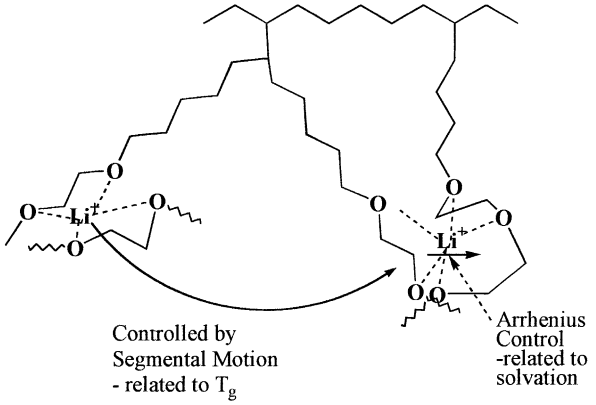


Fig. 3. Schematic representation of the mechanism of ion transport through dry polymers. The presence of the counter anion is not shown.

picture of ion mobility in polymer electrolytes is consistent with recent quasi-elastic neutron scattering measurements on PEO–LiTFSI electrolytes [33], which have detected at least two types of relaxation process. One is consistent with the segmental motion of the polymer while the others are consistent with molecular rearrangements in the solvation shell of the lithium ion. The results shown in Fig. 1 are consistent with control of the ionic motion at low temperature being dominated by segmental motion and hence, the architecture of the polymer while at high temperatures the solvation sphere and the transition state for ionic motion is dominant. Since all of the polymers in Fig. 1 solvate the lithium ions by ethylene oxide units, the convergence of the conductivities indicates that the ion transfer from one solvating chain to another dominates at high temperature.

It is of interest to use molecular models to predict polymer structures that might provide higher mobilities. Ouantum chemical studies on the binding and transition state energies have been carried out by Curtiss and co-workers who have calculated the binding energies of a number of solvation schemes [34–36]. They have found the maximum binding energies for a co-ordination number of five to six oxygens

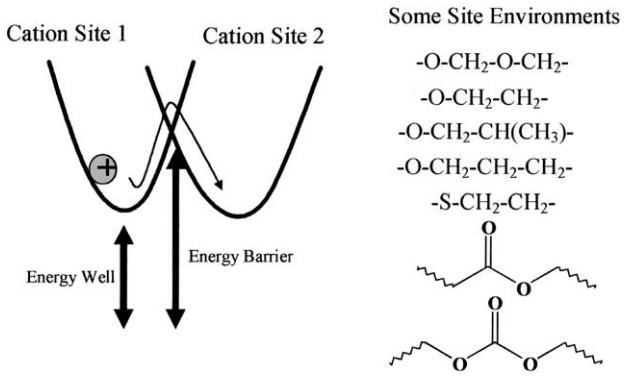


Fig. 4. Schematic representation of the energy wells related to lithium ion solvation and the energy barrier for ion transport from one chain site to another. A number of typical chain structural units are shown: oxymethylene, ethylene oxide, propylene oxide, trimethylene oxide, ethylene sulfide, acrylate and carbonate.

for PEO type polymers and also for polyoxetane structures (three methylene groups between the donor oxygen atoms (TMO)). The binding energies appear to be the same for both types of structures, although the calculations indicate stronger binding when more than one polymer chain is involved. These workers have further attempted to calculate the height of the energy barrier to ion transfer shown in Fig. 4 based on a transition state that involves a decrease in the lithium ion co-ordination number. These calculations indicate that the barrier to ionic motion is lower for the TMO-based polymers and also for mixed EOTMO polymers that contain the ethylene oxide unit as well as the trimethylene oxide units [37]. Such mixed structures were included as experience with metal complexes from analogous polyalkylpolyamines [38,39] has shown that the binding constant may decrease too much in the TMO only polymers and reports from the early polymer electrolyte literature indicated that lithium salts did not dissolve in polyoxetane. So far, the calculations do not indicate that the binding energies are impaired by the presence of the TMO groups.

A good test of these models is provided by comparison of a number of polymer electrolytes which contain different solvation groups of the types shown in Fig. 4. Carbonate and acrylate groups are expected to bind lithium ions too strongly. Propylene oxide is also expected to bind lithium ions strongly and this has been confirmed by conductivity and transport measurements on PPO electrolytes, which show distinctly lower conductivities [17,40] (Fig. 5). In order to test the hypotheses concerning the TMO structures, a series of polymers have been synthesized that contain TMO and mixed TMO–EO groups in the side chains of polyepoxide ethers. The synthesis procedures for the monomers and the polymers are illustrated in Figs. 6 and 7. Fig. 5 shows the conductivities of a series of polymer electrolytes plotted as a function of $1/T$ and clearly show that introduction of units such as carbonate not only lower the overall conductivity but also change the temperature dependence. The most severely affected structure is the comb structure that contains propylene oxide side chains. This polymer also contains acrylate groups in the backbone. However, in the case of the carbonate containing polymer there is one carbonate spaced between three ethylene oxide units and this also appears to be sufficient to severely reduce the conductivity.

The TMO-based polymer electrolytes do not show increased conductivity as would be expected from the quantum calculations and the arguments given above. In fact, in one case denoted $PEPE_1P_1$, the conductivity is over half an order of magnitude lower than the corresponding ethylene oxide polymer, $PEPE_2$ (Figs. 5 and 8). One possible explanation could be that the dielectric constant of the polymer is reduced by the introduction of the extra methylene group but this is not consistent with the increase in conductivity as more trimethylene groups are introduced (Fig. 8). A more consistent explanation would be that there is indeed an increase in the lability of the lithium ion

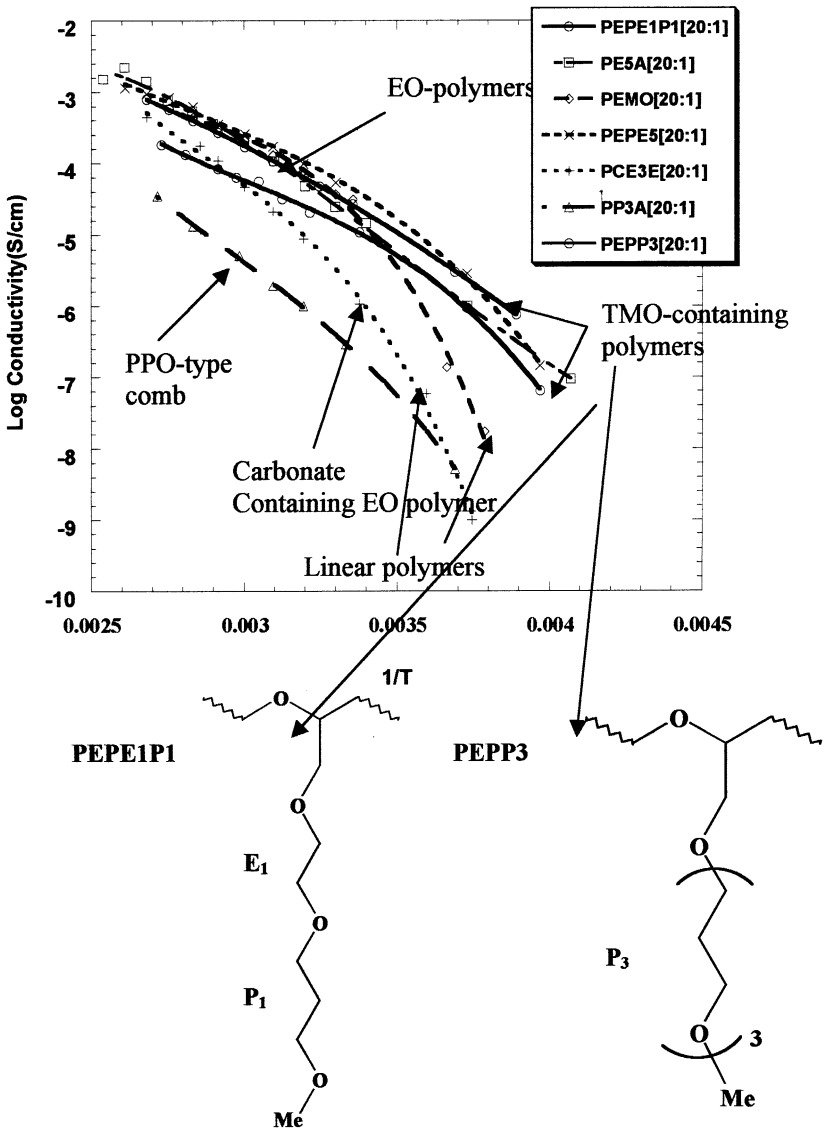


Fig. 5. Conductivities plotted against $1/T$ of a variety of polymers containing the structural groups shown in Fig. 4. LiTFSI salt (20:1).

complexes which may be accompanied by a lowering of the binding energy but that the presence of the propylene oxide unit in the backbone of the polymer serves as a coulombic trap for the lithium ions. The TMO containing polymers show better conductivity at very low temperatures than the EO containing polymers and this is also consistent with the $T_g$ values, which are considerably lower (up to 30 °C) for the TMO polymers at higher concentrations of salt. Full details of these properties will be reported in a future publication. Thus, it is expected that higher conductivities will be attained with polymers that have longer side chains thereby diminishing the impact of the backbone. This behavior was observed for EO containing polymers with acrylate, vinyl or styrene backbones [15,18,19]. A more complete test of the model will be to build polymer architectures that avoid coulombic traps such as propylene oxide units and the synthesis of suitable polymers is ongoing at this laboratory. However, the experiments reviewed here show that there is considerable scope for improvement in lithium ion transport by variation of the nature of the solvation groups involved and that this improvement can be guided by molecular models.

### 3.2. Effect of the salt anion

The discussion so far has ignored the effects of the anion. The TFSI anion is a large anion that effectively delocalizes the negative charge over its structure. The extent of ion pairing is minimized in polymers containing this salt. The transport properties of lithium triflate ($LiCF_3SO_3$) are significantly poorer in PEMO and PEO [17] and this is thought to be due to less delocalization of the charge on the anion with a consequent increase in ion pairing to the lithium ion. Quantum calculations of the binding energies between the lithium ions and anions show lower binding for the TFSI anion than the triflate (Tf). [34] There have been many reports of spectral and electrochemical measurements on the

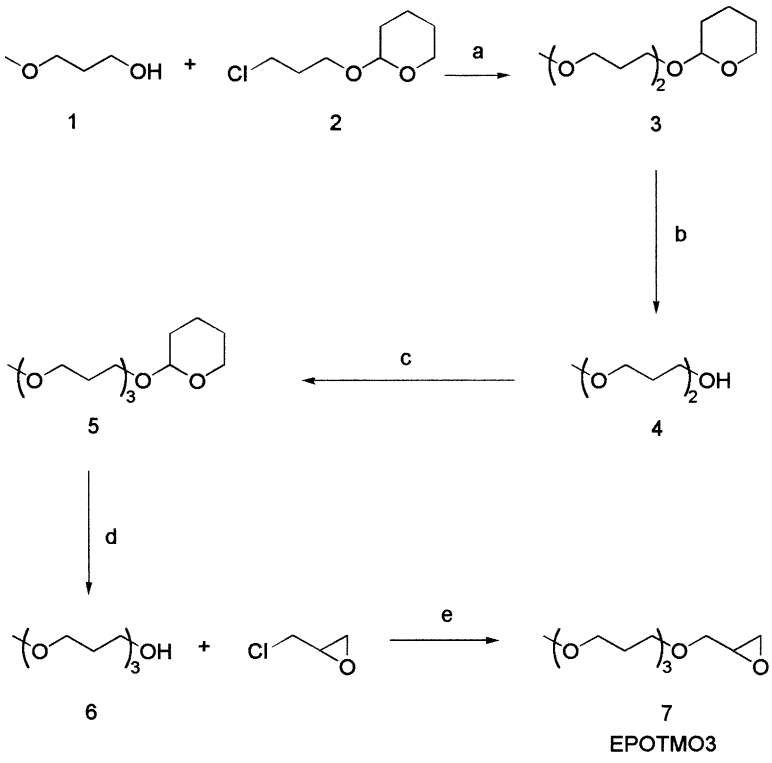


a) NaOH/$H_2O$ (50/50), tetrabutylamonium hydrogen sulfate (THS), Toluene;
b) Ethanol, $H_2O$, $H_2SO_4$;
c) 2, NaOH/$H_2O$ (50/50), THS, Toluene;
d) Ethanol, $H_2O$, $H_2SO_4$;
e) NaOH/$H_2O$ (50/50), THS;

Fig. 6. Synthetic route to incorporate TMO units in the polymer monomer. Variations of this method can be used to incorporate any of the structures shown in Fig. 4.

Tf systems and the effect of the poorer transport properties have been demonstrated to lead to increased capacity fading in cycled cells [41] and to more rapid dendrite growth at lithium electrodes [15]. Andrei et al. [19] measured conductivities for the PEP polyepoxide combs with Tf, perchlorate and $BF_4$ anions and reported little variation with salt identity. However, they did report some variation with side chain length with lithium perchlorate [18,19]. Our

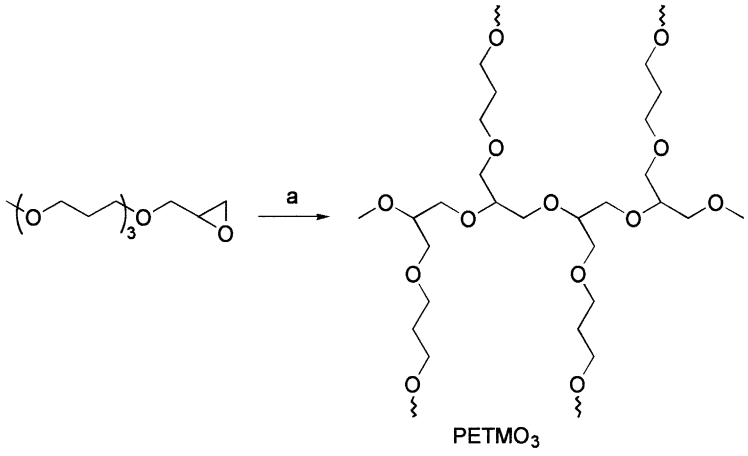


a) 1 M K*t*-OBu in THF, 2%; allyl glycidyl ether, 5%.

Fig. 7. Anionic polymerization conditions used to obtain comb branch polyepoxide ethers.

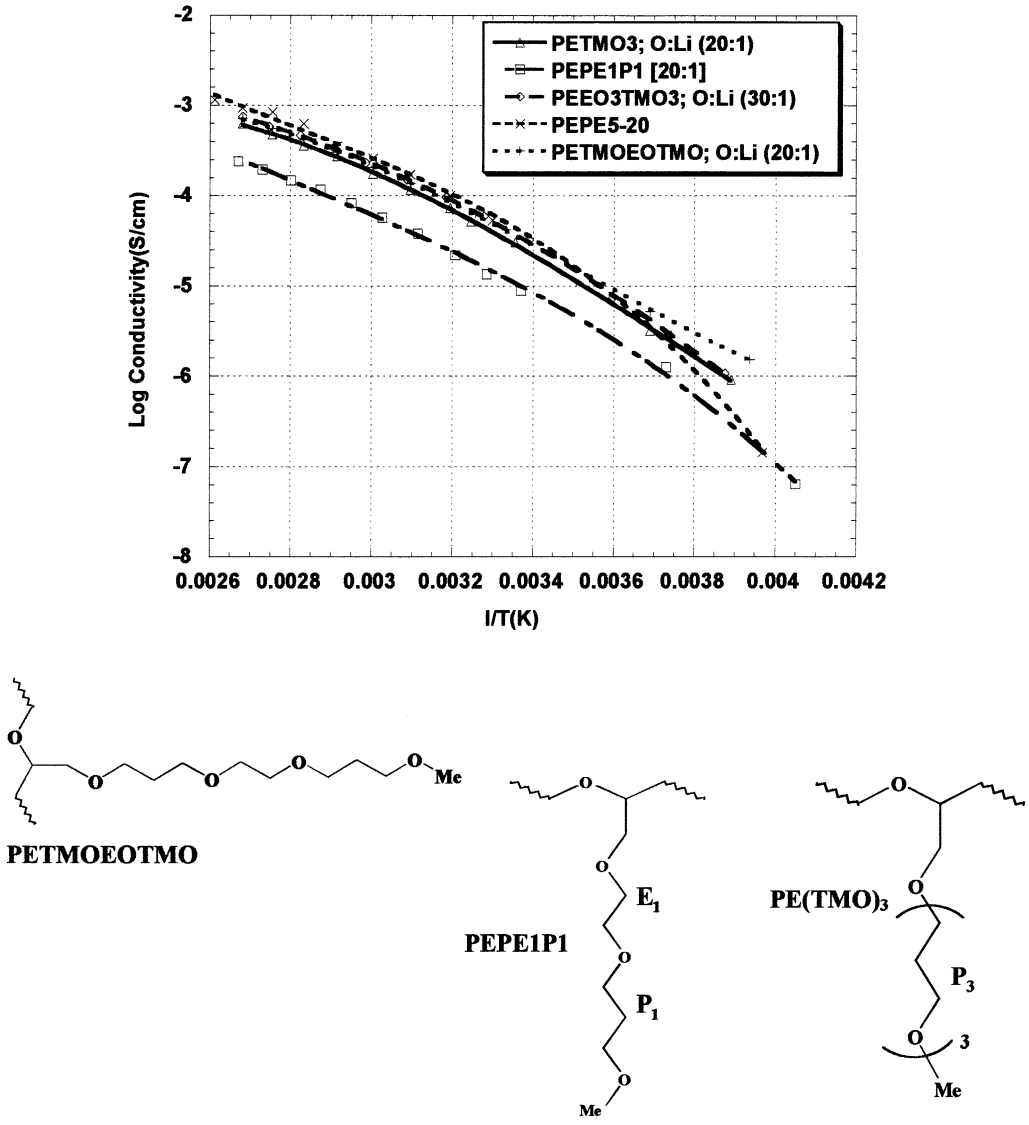


Fig. 8. Conductivities plotted against $1/T$ of a variety of TMO containing polymers with LiTFSI as salt (20:1).

measurements on these polymers with LiTFSI show no variation with side chain length from two to five ethylene oxide units and the conductivity of the $PEPE_5$–LiTFSI electrolyte is shown in Fig. 8. Replacement of the LiTFSI with LiTf confirms the results of Andrei with regards to side chain length. Fig. 9 shows the variation of conductivity of the $PEPE_n$ polymers with $n = 2$–5 and with LiTf. Most interestingly, the conductivities of the longer chain lengths (four and five) are equal to the performance of the polymer electrolytes with LiTFSI salt and confirm the literature report. Since the salt cost of LiTFSI is very high, this result provides an approach to lowering the salt cost but yet maintaining performance for EV use.

It is interesting to note that the highest conductivities are obtained at a side chain length of four EO units. This corresponds to five oxygens in a single side chain and may indicate that the lithium ion is bound to a single side chain. At shorter side chain length the lithium ion is forced to bind to more than one chain. It may well be true that the ion pairing of the anion may form a cross-link between chains that impairs the movement of the lithium ion. An alternative explanation is that the propylene oxide oxygen in the backbone may play a more important role at shorter side chain length with LiTf. Clearly, there is much scope for modeling of the behavior of these structures and most encouragingly the experimental data already provides intriguing possibilities for matching theory and experiment. The observed effect of the salt and the postulated coulombic trap effect of units such as propylene oxide or acrylate, demonstrate the need to model the whole system on the molecular level and not just selected parts.

### 3.3. Effect of surfaces

Transport processes of liquids and polymers adjacent to solid surfaces are considerably altered from those found in

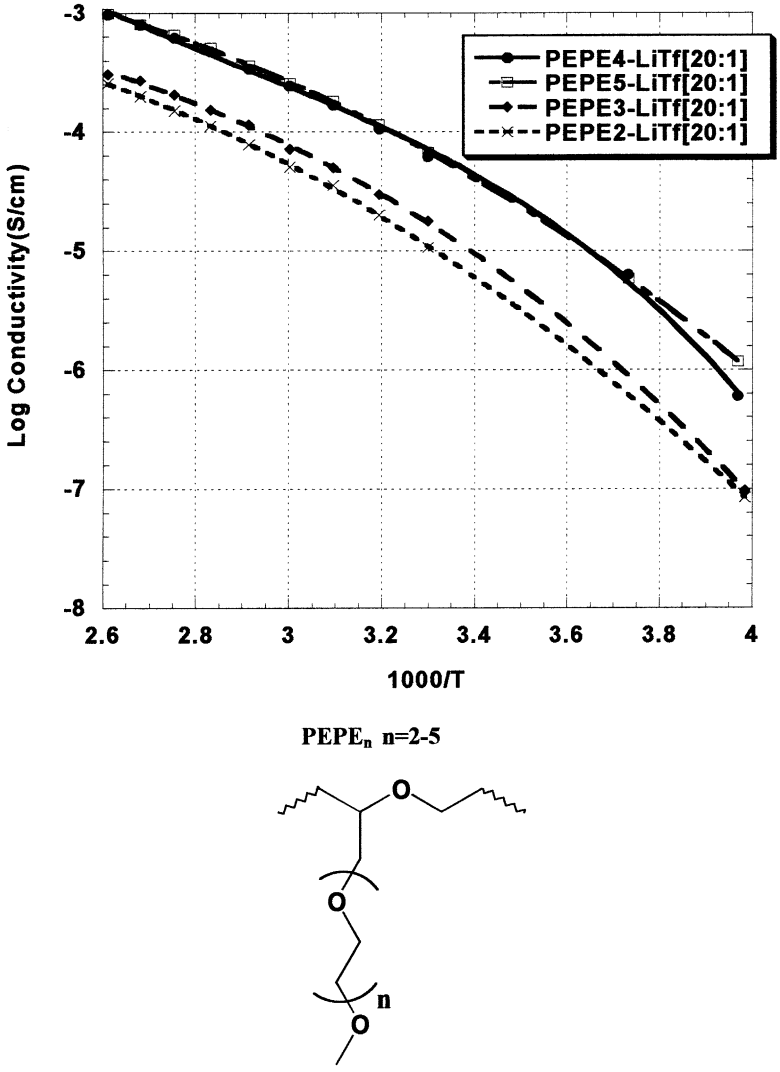


Fig. 9. Conductivities of polyepoxide ethers of various side chain length (two to five ethylene oxide units) with LiTf salt (20:1).

the bulk whether or not there are any specific interactions with the surface as would be the case with an electrode. For large polymers the freedom of movement of the chain is impeded by the solid and consequently the segmental motion should be reduced, indicating a rise in the $T_g$ value. Indeed, such behavior has been reported for filled polymers by Eisenberg who observed the presence of two glass transition temperatures in various polymers filled with nanoparticles of filmed silica [42,43]. The second $T_g$ could be as much as 100 K higher in temperature than the first one. The observations were consistent with NMR relaxation time measurements [44] and recent neutron scattering experiments that have detected two different types of relaxation phenomena in the presence of filler particles [45]. The observation of the second $T_g$ is dependent upon the chemical nature of the polymer, its molecular weight, the strength of the interaction of the polymer with the particle and the amount of filler in the polymer. Typically, the second $T_g$ is most easily observed at 10% filler loading using dynamic mechanical analysis. As the proportion of filler material is increased the second $T_g$ shifts in magnitude and temperature.

The behavior reported by Eisenberg is rationalized by a model that postulates an immobile layer of polymer next to the solid particle with a second layer of polymer further out that is restricted in its motion. As the proportion of filler particles is increased, the volume of restricted polymer increases through overlap and the second glass transition is observed. Further addition of filler particles leads to more polymer in the completely immobile form, which does not have a glass transition. This model of filled polymer behavior can be applied to battery electrolytes in separators and composite electrodes. Recently, there has been much interest in the effects of added filler nanoparticles upon the transport properties of PEO–lithium salt electrolytes [46–51]. The most striking effect of the addition of fillers is the inhibition of crystallization of the PEO and the conductivity at 25 °C rises to the same levels as PEMO shown in Fig. 1 upon addition of 10% $Al_2O_3$ and $TiO_2$ nanoparticles. The use of inexpensive fillers appears to be a more cost-effective way to

reduce the crystallinity of PEO electrolytes than the more involved co-polymerizations with propylene oxide and oxymethylene groups. Filler particles are also useful for altering the mechanical properties of polymers and liquids. These observations are compatible with the Eisenberg model as the particles impede the segmental motion so that the polymer chains are unable to reach the conformations required for crystallization.

It has been noted, however, that there is an increase in conductivities above the levels of the ceramic-free electrolyte in temperature regions where crystallinity is not an issue. Assuming this is not an artifact of adventitious water entrained in the filler this observation has been rationalized by specific interactions between the polymer and the filler particles that may facilitate alternative mechanisms of ion transport. Recent NMR measurements of PEO–ceramic electrolytes have shown evidence for less segmental motion of the polymer and yet higher lithium ion diffusivity [51]. These observations are consistent with the Eisenberg model, which predicts restricted segmental motion and an increase in free volume due to the restricted polymer motion. Eisenberg reported that the thermal history and annealing of polymer–ceramics mixtures had a considerable effect upon the second glass transition. An increase in free volume of the polymer may allow more rapid diffusion of the lithium ions, particularly if they are ion-paired with the anion. It is noted that a recent report on PEO and PEMO with LiTFSI salts has shown no beneficial effect on conductivity aside from inhibition of crystallinity [50]. Simple experiments such as investigation of thermal history [52,53] are possible to shed more light on these issues and, in particular, the wealth of rheological data and models is a source of assistance in the prediction of behavior.

The Eisenberg model possibly has even more relevance with electrodes. Although typical cathode particles in composite cathodes have dimensions much larger than nanoparticles, they are connected electronically by carbon nanoparticles that can provide similar conditions regarding restriction of segmental motion of polymers as the ceramic nanoparticles described above. Clearly, surface roughness and pores in the cathode particles will also have an effect. It is therefore likely that transport properties within porous electrodes will differ somewhat from those observed in the bulk separator. Account is taken of changes in transport properties in the electrode in porous electrode theory by use of the Bruggeman correction which is used to adjust for tortuosity [11,54,55] but also accounts for differences in transport properties due to the presence of the surface. The Eisenberg model is applicable to composite electrodes in both polymer and lithium ion batteries and provides a physical basis to justify use of adjustable parameters in battery system models. A further consequence of the Eisenberg model is that changes in the polymer such as cross-linking will lead to changes in the effective transport properties in the electrode during the life of the battery. Poorer transport properties can lead to lower capacities [41] and hence, changes in the electrolyte may lead to capacity fade that is unrelated to any internal changes in the electrode material.

The Eisenberg model of an immobilized layer immediately on the surface with a restricted transport layer adjacent to this that extends out into the bulk of the electrolyte bears considerable resemblance to the models of the solid electrolyte interface proposed by many for the lithium and carbon anodes [56–58]. The impedance behavior typically ascribed to irreversible reactions may in fact by due to these layers. However, the model clearly implies a change in mechanism of ion transport close to the electrode surface since the segmental motion of the polymer is impeded. In fact, directly adjacent to the electrode is a glassy layer of polymer which may extend out into the electrolyte for tens of nanometers depending on the nature of the polymer–electrode interaction and the mechanical properties of the polymer which derive from the polymer structure, salt concentration and identity plus the presence of impurities, side reaction products or additives that form a surface layer. Variations in the structure of the polymer solvation groups such as the ones outlined above may well affect the transport through these layers. Since it was noted in the system modeling that the anode resistance could strongly affect power and energy densities, these molecular considerations can have profound impacts on the battery performance.

The model is obviously relevant to the complicated problem of dendrite growth at lithium metal electrodes. Mechanical properties of the electrolyte have been shown to play a significant role in this phenomenon. While low capacity cycling (0.35 C/cm$^2$) of PEMO-LiTFSI at 85 °C gives hundreds of cycles with no sign of dendrites at current densities well below the limiting current, the same electrolyte showed signs of dendrites after only two high capacity cycles (1.4 C/cm$^2$). By contrast, cross-linked PEPE$_2$–LiTFSI sustained progressively longer cycling without dendrites as a function of the mechanical properties. Fig. 10 shows the cycling of cross-linked PEPE$_2$–LiTFSI in lithium/lithium cells. The 5% cross-linked polymer electrolyte had an elastic modulus of $10^4$ Pa and sustained 15 cycles (21.6 C/cm$^2$) before a short circuit developed. The 10% cross-linked polymer electrolyte had an elastic modulus of $10^5$ Pa and sustained 102 cycles (150 C/cm$^2$) before failure. In both cases, the failure was quite sudden with no sign of noisy voltage behavior that appeared with the viscous liquid PEMO electrolyte ($M_w$ 150 k). The Eisenberg model provides some insight into how the polymer may behave at the surface of the electrode to restrain the dendrite growth due to mechanical reasons and also promote it due to transport properties. Measurements of polymer electrolyte mechanical properties with nanoparticles may give valuable insights into the nature of the surface layers that could be difficult to obtain otherwise.

One conclusion to be drawn is that the desired mechanical properties of the polymer are different depending upon the electrode. For lithium anodes, a highly cross-linked polymer

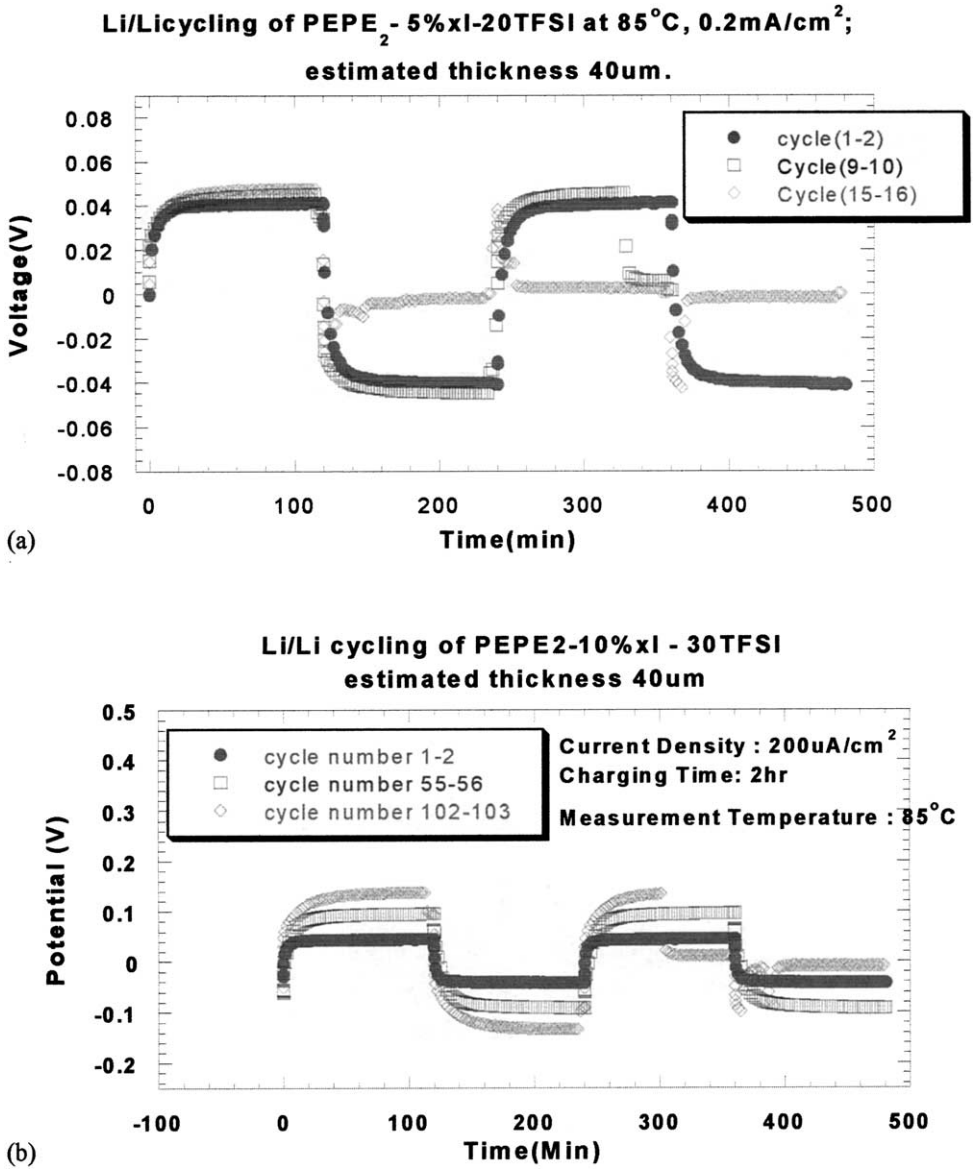


Fig. 10. Galvanostatic cycling behavior of lithium/lithium symmetrical cells with cross-linked $PEPE_2$–LiTFSI electrolytes. Conditions given on the figure. Polymer in (a) was 5% cross-linked and had an elastic modulus of $10^4$ Pa. Polymer in (b) was 10% cross-linked and had an elastic modulus of $10^5$ Pa.

that still does not impair ion transport is desired. For composite electrodes, a minimum of cross-linking is desired that is compatible with mechanical strength and the transport properties. There are implications with regards to how side reactions may change these properties over time and life cycle and hence influence the battery performance over time.

### 3.4. Effect of side reactions

Side reactions may occur at the electrodes or may be due to inherent instability of the cell components themselves. For example, the typical electrolyte used in lithium ion batteries is inherently unstable due to the presence of Lewis acids arising from the use of $LiPF_6$ [59]. Indeed, experiments in this laboratory have shown that ether polymers such as PEO are also unstable to Lewis acids. Addition of $LiPF_6$ to PEGDME 250 led to distinct changes in the molecular weight distribution due to both chain scission and chain formation. Acids may also be formed by overcharging at cathodes and these acid species may result in changes in the molecular weight distribution of the polymer within the electrode. As noted above, the transport properties of the electrolyte in the cathode may then be altered and the cell capacity change as a result. One can note that propylene oxide units used to prevent crystallinity, to provide cross-linkable points or to form comb structures are more susceptible to oxidation or acid catalyzed reactions. Chain scission is expected at the anode [60,61] which may result in a weakening of the mechanical properties of the electrolyte and consequent growth of dendrites. This may be the cause of the failure observed in Fig. 10.

The effects of side reactions can thus be related to changes in mechanical and morphological properties of the electrolytes at the interfaces. These in turn can be related to the transport properties both in the interfacial layers and in the bulk of the electrolytes. Models of these processes can thus be used to provide data that may be used in system models of the battery performance. Thus, the effect of side reactions on the evolution of the battery calendar and life cycle can be predicted provided the appropriate mechanical and morphological models are used. Finally the models of ion transport and chemical reactivity can be used to provide design parameters to aid in the synthesis of new and better materials that will achieve the performance and lifetime required for EV use. Relatively simple kinetic measurements of side reactions can be used to provide a basis for lifetime estimates provided that the consequences of these reactions can be linked through the intermediate models to the battery performance. It is also noted that although the transport properties required of polymer electrolytes for EV performance may be attained by operation at high temperatures, there will be an increase in the rate of side reactions both at the electrodes and in the bulk electrolyte. These reactions may ultimately limit the calendar and life cycle and may justify the continued search for more conductive and stable electrolyte systems.

## References


[1] M. Armand, J.Y. Sanchez, M. Gauthier, Y. Choquette, in: J. Lipkowski, P.N. Ross (Eds.), Electrochemistry of Novel Materials, VCH, New York, 1994, p. 65.
[2] M. Armand, Solid State Ionics 69 (1994) 309.
[3] N.H. Ge, C.M. Wong, R.L. Lingle, J.D. McNeill, K.J. Gaffney, C.B. Harris, Science 279 (1998) 202.
[4] M. Armand, Faraday Discuss. Chem. Soc. (1989) 65.
[5] J.W. Halley, Y. Duan, L.A. Curtiss, A.G. Baboul, J. Chem. Phys. 111 (1999) 3302.
[6] O. Borodin, G.D. Smith, R.L. Jaffe, J. Comput. Chem. 22 (2001) 641.
[7] M.A. Ratner, P. Johansson, D.F. Shriver, MRS Bull. 25 (2000) 31.
[8] M.A. Ramer, in: J.R. MacCallum, C.A. Vincent (Eds.), Polymer Electrolyte Reviews. Part I, Elsevier, London, 1987, p. 173.
[9] K.E. Thomas, S.E. Sloop, J.B. Kerr, J. Newman, J. Power Sources, this issue.
[10] M. Doyle, J. Newman, J. Appl. Electrochem. 27 (1997) 846.
[11] M. Doyle, J. Newman, Electrochim. Acta 40 (1995) 2191.
[12] M. Doyle, J. Newman, J. Power Sources 54 (1995) 46.
[13] P.P. Simon, H.J. Ploehn, J. Rheol. 41 (1997) 641.
[14] Y. Rouault, K. Kremer, J. Chem. Phys. 111 (1999) 3288.
[15] O. Buriez, Y.B. Han, J. Hou, J.B. Kerr, J. Qiao, S.E. Sloop, M.M. Tian, S.G. Wang, J. Power Sources 89 (2000) 149.
[16] Y.P. Ma, M. Doyle, T.F. Fuller, M.M. Doeff, L.C. De Jonghe, J. Newman, J. Electrochem. Soc. 142 (1995) 1859.
[17] M.M. Doeff, L. Edman, S.E. Sloop, J. Kerr, L.C. De Jonghe, J. Power Sources 89 (2000) 227.
[18] L. Marchese, M. Andrei, A. Roggero, S. Passerini, P. Prosperi, B. Scrosati, Electrochim. Acta 37 (1992) 1559.
[19] M. Andrei, A. Roggero, L. Marchese, S. Passerini, Polymer 35 (1994) 3592.
[20] H.R. Allcock, D.E. Smith, Y.B. Kim, J.J. Fitzgerald, Macromolecules 27 (1994) 5206.
[21] D.J. Wilson, C.V. Nicholas, R.H. Mobbs, C. Booth, Br. Polym. J. 22 (1990) 129.
[22] A. Vallee, M. Duval, F. Brochu, M. Kono, E. Hayashi, T. Sada, US Patent no. 5,755,985, 1998.
[23] D.W. Dees, V.S. Battaglia, L. Redey, G.L. Henriksen, R. Atanasoski, A. Belanger, J. Power Sources 89 (2000) 249.
[24] L. Edman, A. Ferry, M.M. Doeff, J. Mater. Res. 15 (2000) 1950.
[25] L. Edman, M.M. Doeff, A. Ferry, J. Kerr, L.C. De Jonghe, J. Phys. Chem. B 104 (2000) 3476.
[26] M. Gauthier, A. Belanger, P. Bouchard, B. Kapfer, S. Ricard, G. Vassort, M. Armand, J.Y. Sanchez, L. Krause, J. Power Sources 54 (1995) 163.
[27] K.L. Heitner, J. Power Sources 89 (2000) 128.
[28] J.W. Halley, Y. Duan, B. Nielsen, P.C. Redfern, L.A. Curtiss, J. Chem. Phys. 115 (2001) 3957.
[29] J.W. Halley, P. Schelling, Y. Duan, Electrochim. Acta 46 (2000) 239.
[30] J.W. Halley, Y.H. Duan, J. Power Sources 89 (2000) 139.
[31] M.A. Ratner, D.F. Shriver, MRS Bull. (1989) 39.
[32] J.F. Snyder, M.A. Ratner, D.F. Shriver, J. Electrochem. Soc. 148 (2001) A858.
[33] G.M. Mao, R.F. Perea, W.S. Howells, D.L. Price, M.L. Saboungi, Nature 405 (2000) 163.
[34] L.A. Curtiss, October 2000, personal communication.
[35] A.G. Baboul, P.C. Redfern, A. Sutjianto, L.A. Curtiss, J. Am. Chem. Soc. 121 (1999) 7220.
[36] A. Sutjianto, L.A. Curtiss, J. Phys. Chem. A 102 (1998) 968.
[37] L.A. Curtiss, J. Power Sources 110 (2) (2002) 401–405.
[38] P. Osvath, D.C. Weatherburn, W.T. Robinson, Trans. Met. Chem. 16 (1991) 344.
[39] R.D. Hancock, A.E. Martell, Chem. Rev. 89 (1989) 1875.
[40] S.E. Sloop, M.M. Doeff, O. Buriez, J.B. Kerr, in preparation.
[41] M.M. Doeff, A. Ferry, Y.P. Ma, L. Ding, L.C. De Jonghe, J. Electrochem. Soc. 144 (1997) L20.
[42] G. Tsagaropoulos, A. Eisenberg, Macromolecules 28 (1995) 396.
[43] G. Tsagaropoulos, A. Eisenberg, Macromolecules 28 (1995) 6067.
[44] J. O'Brien, E. Cashell, G.E. Wardell, V.J. McBrierty, Macromolecules 9 (1976) 653.
[45] S. Gagliardi, V. Arrighi, R. Ferguson, M.T.F. Telling, Phys. B 301 (2001) 110.
[46] B. Kumar, L.G. Scanlon, J. Power Sources 52 (1994) 261.
[47] B. Kumar, L.G. Scanlon, J. Electroceram. 5 (2000) 127.
[48] F. Croce, G.B. Appetecchi, L. Persi, B. Scrosati, Nature 394 (1998) 456.
[49] F. Croce, R. Curini, A. Martinelli, L. Persi, F. Ronci, B. Scrosati, R. Caminiti, J. Phys. Chem. B 103 (1999) 10632.
[50] P. Johansson, M.A. Ratner, D.F. Shriver, J. Phys. Chem. B 105 (2001) 9016.
[51] S.H. Chung, Y. Wang, L. Persi, F. Croce, S.G. Greenbaum, B. Scrosati, E. Plichta, J. Power Sources 97/98 (2001) 644.
[52] B. Kumar, L.G. Scanlon, Solid State Ionics 124 (1999) 239.
[53] B. Kumar, L.G. Scanlon, R.J. Spry, J. Power Sources 96 (2001) 337.
[54] M. Doyle, J. Newman, A.S. Gozdz, C.N. Schmutz, J.M. Tarascon, J. Electrochem. Soc. 143 (1996) 1890.
[55] J. Newman, Electrochemical Systems, Prentice-Hall, Englewood Cliffs, NJ, 1991.
[56] D. Aurbach, J. Power Sources 89 (2000) 206.
[57] D. Fauteux, Electrochim. Acta 38 (1993) 1199.
[58] D. Aurbach, E. Zinigrad, H. Teller, P. Dan, J. Electrochem. Soc. 147 (2000) 1274.
[59] S.E. Sloop, J.K. Pugh, S. Wang, J.B. Kerr, K. Kinoshita, Electrochem. Solid State Lett. 4 (2001) A42.
[60] J.B. Kerr, J. Electrochem. Soc. 132 (1985) 2839.
[61] D. Aurbach, A. Zaban, Y. Gofer, O. Abramson, M. Benzion, J. Electrochem. Soc. 142 (1995) 687.